Scripta Materialia 154 (2018) 127–130

Contents lists available at ScienceDirect

Scripta Materialia

journal homepage: www.elsevier.com/locate/scriptamat

Regular article

Exploring the accuracy limits of lattice strain quantification with synthetic diffraction data

C. Zhang, T.R. Bieler, P. Eisenlohr*

Chemical Engineering and Materials Science, Michigan State University, East Lansing, MI 48824, USA

ARTICLE INFO

Article history:
Received 9 March 2018
Received in revised form 16 May 2018
Accepted 19 May 2018
Available online xxxx

Keywords:
Differential aperture X-ray microscopy (DAXM)
Lattice deformation gradient
Least-squares regression
COBYLA

ABSTRACT

From a collection of scattering vectors obtained by synchrotron X-ray diffraction, the lattice strain can be spatially quantified. This paper explores the inherent accuracy limits by comparing a least-squares regression and an optimization method applied to synthetic diffraction data excluding any measurement uncertainties potentially present in real experiments. The optimization method in combination with a novel fitness function can identify the deviatoric/full lattice deformation gradient with accuracy better than 10^{-9}. The least-squares regression is much less accurate unless all scattering vector lengths are known, in which case the exact lattice deformation gradient can be recovered.

Quantitative experimental characterization of lattice strain with high spatial resolution provides important information about internal defects and strains at the microscale. Several experimental techniques have been developed to fulfill this need, such as high-resolution electron backscattering diffraction (HREBSD) [1], neutron diffraction [2], and synchrotron X-ray based diffraction strategies [3-7]. Among these methods, one type of synchrotron X-ray based diffraction, differential aperture X-ray microscopy (DAXM), is commonly used to non-destructively characterize subsurface lattice strain with high spatial resolution using various numerical optimization techniques, denoted as the strain quantification in this letter. The lattice strain uncertainty has been equated to the variation ($\pm 10^{-4}$) observed for the deviatoric strain tensor components extracted from a nominally strain-free Si single crystal [8]. The source of this uncertainty is often speculated as the uncertainty of the peak position on the detector [9] or the limited reciprocal space coverage due to small detector size [10]. However, the exact source of the uncertainty in the extracted lattice strain has rarely been discussed, leaving the possibility that other sources, such as the numerical optimization process, could also contribute to the reported value. The objective of this letter is to analyze the uncertainty connected to numerical optimization, which is a fundamental part of a systematic investigation of uncertainty sources for strain quantification. A direct method based on least-squares regression (L2) and an iterative optimization based method (opt) are compared regarding their accuracy in extracting (deviatoric) lattice deformation gradients from virtual DAXM experiments, thus elucidating whether the choice of the strain quantification method is an important concern.

In the classic diffraction theory, the basis $\mathbf{B}_0 = [\mathbf{a}_0, \mathbf{b}_0, \mathbf{c}_0]$ of a strain-free crystal can transform to a deformed basis

$$\mathbf{B} = \mathbf{F}\,\mathbf{B}_0 \tag{1}$$

due to a continuous elastic distortion characterized by the deformation gradient $\mathbf{F}$. For such a strained lattice, the scattering vectors $\mathbf{q}^{(i)}$ where each $i = 1, 2, \ldots, N$ is associated with a diffracting plane having Miller indices $\mathbf{n}^{(i)} = (h\,k\,l)^{(i)}$, are given by the difference between the incident wavevector $\mathbf{k}_0^{(i)}$ and diffracted wavevector $\mathbf{k}^{(i)}$ in reciprocal space as

$$\mathbf{k}^{(i)} - \mathbf{k}_0^{(i)} = \mathbf{q}^{(i)} = \mathbf{B}^{\star}\mathbf{n}^{(i)}$$

or expressed in terms of real space quantities[1] as

$$\begin{aligned}\mathbf{k}^{(i)} - \mathbf{k}_0^{(i)} = \mathbf{q}^{(i)} &= 2\pi\mathbf{B}^{-\mathrm{T}}\mathbf{n}^{(i)} \\ &= 2\pi(\mathbf{F}\mathbf{B}_0)^{-\mathrm{T}}\mathbf{n}^{(i)} \\ &= \mathbf{F}^{-\mathrm{T}}2\pi\mathbf{B}_0{}^{-\mathrm{T}}\mathbf{n}^{(i)}.\end{aligned} \tag{2}$$

* Corresponding author.
E-mail address: eisenlohr@egr.msu.edu (P. Eisenlohr).

[1] A basis $\mathbf{B}$ transforms to reciprocal space as $\mathbf{B}^{\star} = 2\pi\mathbf{B}^{-\mathrm{T}}$, *i.e.* the inverse of the transpose of $\mathbf{B}$ times 2π.

https://doi.org/10.1016/j.scriptamat.2018.05.028
1359-6462/

Thus, scattering vectors of the distorted lattice can be calculated from their undistorted counterparts $\mathbf{q}_0$ if the deformation gradient $\mathbf{F}^{-\mathrm{T}} = \mathbf{F}^{\star}$ is known:

$$\mathbf{q}^{(i)} = \mathbf{F}^{\star}\ \mathbf{B}_0{}^{\star}\mathbf{n}^{(i)} = \mathbf{F}^{\star}\ \mathbf{q}_0^{(i)} \tag{3a}$$

or in matrix form $\mathbf{M} = \mathbf{F}^{\star}\ \mathbf{M}_0$, (3b)

where $\mathbf{M} = [\mathbf{q}^{(1)}, \mathbf{q}^{(2)}, \ldots, \mathbf{q}^{(N)}]$ and $\mathbf{M}_0 = \left[\mathbf{q}_0^{(1)}, \mathbf{q}_0^{(2)}, \ldots, \mathbf{q}_0^{(N)}\right]$. Conversely, the deformation gradient that causes observed deviations between $\mathbf{q}_0^{(i)}$ and $\mathbf{q}^{(i)}$ can be uniquely determined from any set of three linearly independent scattering vectors $\mathbf{q}_0^{(1,2,3)}$ and their corresponding $\mathbf{q}^{(1,2,3)}$ through inversion of $\mathbf{M}_0$, *i.e.*

$$\mathbf{F}^{\star} = \mathbf{M}\mathbf{M}_0{}^{-1}.$$

In the case of noisy scattering vectors, the deformation gradient can be found from all (three or more) scattering vectors using least-squares regression (L2):

$$\mathbf{M}\ \mathbf{M}_0{}^{\mathrm{T}} = \mathbf{F}^{\star}\ \mathbf{M}_0\mathbf{M}_0{}^{\mathrm{T}}$$
$$\mathbf{F}^{\star} = \left(\mathbf{M}\ \mathbf{M}_0{}^{\mathrm{T}}\right)\left(\mathbf{M}_0\mathbf{M}_0{}^{\mathrm{T}}\right)^{-1}. \tag{4}$$

Up to this point, it was tacitly assumed that *all* scattering vectors have a measured length, *i.e.*, the incident wavelength that is causing the diffraction is known. However, the area detector technology in current use does not identify the wavelength of incident photons in each diffraction peak. Without knowledge of the wavelength, only the direction but not the absolute magnitude of scattering vectors can be established. In other words, the standard DAXM experiment can only characterize which set of parallel lattice planes are diffracting, but not their associated spacing. Consequently, the unit cell distortion, which can be expressed as the lattice deformation gradient $\mathbf{F}$ extracted from white-beam DAXM data using strain quantification, is only meaningful in terms of its deviatoric component

$$\mathbf{F}_{\mathrm{D}} = \mathbf{F}/(\det\mathbf{F})^{\frac{1}{3}}. \tag{5}$$

To acquire the full lattice deformation gradient, additional scans using monochromatic X-rays of different energies, commonly referred to as "energy scans", are performed in order to determine the length of n selected scattering vector(s). During such an energy scan, the occurrence of a particular peak of interest is carefully monitored while the energy of the incident beam is incrementally changed. The time required to scan multiple diffraction peaks scales in proportion to n because different diffraction peaks generally do not share the same narrow window of scanned X-ray energy. Consequently, in the more typical case of an unknown scattering vector length $q^{(i)}$, the relationship between a distorted and undistorted scattering vector becomes

$$q^{(i)}\widehat{\mathbf{q}^{(i)}} = \mathbf{F}^{\star}\ q_0^{(i)}\widehat{\mathbf{q}_0^{(i)}}$$
$$\widehat{\mathbf{q}^{(i)}} = \underbrace{\left(\frac{q_0^{(i)}}{q^{(i)}}p^{\star}\right)}_{\substack{\text{individual}\\ \text{correction}\\ \text{factor}}}\mathbf{F}_{\mathrm{D}}{}^{\star}\ \widehat{\mathbf{q}_0^{(i)}}, \tag{6}$$

where $\hat{\mathbf{q}}$ denotes the unit vector ($\|\hat{\mathbf{q}}\| = 1$) aligned with $\mathbf{q}$, and $p^{\star}$ and $\mathbf{F}_{\mathrm{D}}^{\star}$ correspond, respectively, to the spherical (or hydrostatic) and deviatoric parts of $\mathbf{F}^{\star}$. Because $p^{\star}$ becomes obscured by each unknown scattering vector length $q^{(i)}$, it is impossible to deduce the spherical part of $\mathbf{F}^{\star}$ from Eq. (6). For the same reason, using the least-squares regression Eq. (4) on a set of scattering vectors where a part or all are of unit length (such that $\mathbf{M} = \left[\mathbf{q}^{(1)}, \ldots, \mathbf{q}^{(n)}, \widehat{\mathbf{q}^{(n+1)}}, \ldots, \widehat{\mathbf{q}^{(N)}}\right]$ and similarly for $\mathbf{M}_0$) results in a less exact solution for $\mathbf{F}_{\mathrm{D}}^{\star}$ because the individual correction factors that relate Eq. (6) to Eq. (3a) are necessarily dropped.

To find an approximation $\tilde{\mathbf{F}}^{\star}$ to the solution $\mathbf{F}^{\star}$ of Eq. (3a) for the most general case where (only) $n \geq 0$ of the N scattering vectors have measured length, an iterative optimization scheme (opt) implemented in Constrained Optimization by Linear Approximation (COBYLA) with a tolerance of 10^{-14} is used in this study. The function

$$\mathcal{U}^2\left(\tilde{\mathbf{F}}^{\star}\right) = \left[\sum_{i=1}^{n}\left(\left\|\mathbf{q}^{(i)} - \tilde{\mathbf{F}}^{\star}\ \mathbf{q}_0^{(i)}\right\|^2 / \left\|\mathbf{q}^{(i)}\right\|^2\right) + \sum_{i=n+1}^{N}\left\|\widehat{\mathbf{q}^{(i)}} - \widehat{\mathbf{F}^{\star}\ \mathbf{q}_0^{(i)}}\right\|^2\right]/N \tag{7}$$

is designed to penalize relative deviations between the actually observed scattering vectors and those predicted from the assumed $\tilde{\mathbf{F}}^{\star}$.[2] The square root $\mathcal{U}$ is used as fitness function in the optimization scheme to fully utilize the underlying machine precision. In the usual white-beam case where *all* scattering vectors are unit vectors ($n = 0$), the resulting $\tilde{\mathbf{F}} = \tilde{\mathbf{F}}^{\star-\mathrm{T}}$ should be converted to $\tilde{\mathbf{F}_{\mathrm{D}}}$ using Eq. (5).

The assessment of the two methods (L2 and opt) was performed using virtual DAXM experiments that simulate the actual beam and detector geometry at beamline 34-ID-E of the Advanced Photon Source (APS) at the Argonne National Laboratory. The geometry has both the incident beam $\mathbf{k}_0$ (with an energy range of 7 keV to 30 keV) and the overhead area detector with unit normal $\mathbf{n}_{\mathrm{CCD}}$ fixed relative to the lab frame, such that

$$\mathbf{e}_3 \parallel \mathbf{k}_0, \qquad \mathbf{e}_2 \parallel \mathbf{n}_{\mathrm{CCD}}, \qquad \mathbf{e}_1 \parallel (\mathbf{e}_2 \times \mathbf{e}_3)\,.$$

A large number (9.5×10^4) of virtual single crystals with random lattice orientation were placed at the origin of the laboratory frame (see Fig. 1) and distorted by deformation gradients

$$\mathbf{F} = \mathbf{R}\,\mathbf{U}.$$

Each rotation $\mathbf{R}$ is about a random axis with a rotation angle θ chosen from a logarithmically uniform distribution between 0.001° and 0.1°. The (symmetric) stretch

$$\mathbf{U} = (\mathbf{I} + \boldsymbol{\epsilon})_{\mathrm{sym}} = \left((\mathbf{I} + \boldsymbol{\epsilon}) + (\mathbf{I} + \boldsymbol{\epsilon})^{\mathrm{T}}\right)/2$$

is composed from $\mathbf{I}$ (second-order identity tensor) and $\boldsymbol{\epsilon}$ having nine components that are randomly sampled from a logarithmically uniform distribution ranging from 1×10^{-5} to 1×10^{-3}. (The symmetrization of $\mathbf{I} + \boldsymbol{\epsilon}$ biases the expected off-diagonal (shear) components to be slightly larger than the diagonal (normal) components.)

The virtual detector captures signals diffracting from the single crystal within a 45° cone (see Fig. 1). Out of all possible diffracted wavevectors $\mathbf{k}$ those with zero structure factor[3] or with Miller indices (h, k, l) exceeding ±20 are excluded, a condition that is typically observed in beamline 34-ID-E data. As not every collected diffraction peak can necessarily be successfully indexed in a real

[2] Instead of $\tilde{\mathbf{F}}^{\star}$, the better conditioned $\tilde{\mathbf{F}}^{\star} - \mathbf{I}$ is selected as the quantity to be optimized.

[3] Here based on face-centered cubic lattice for simplicity.

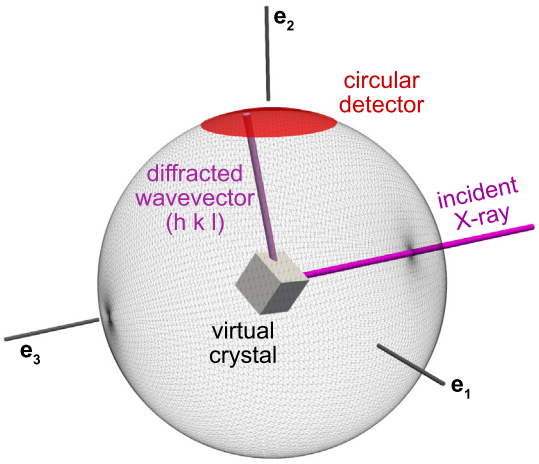

Fig. 1. Schematics of the virtual diffraction configuration. The red cap represents the circular detector covering a 45° detecting range similar to the setup at beamline 34-ID-E at APS.

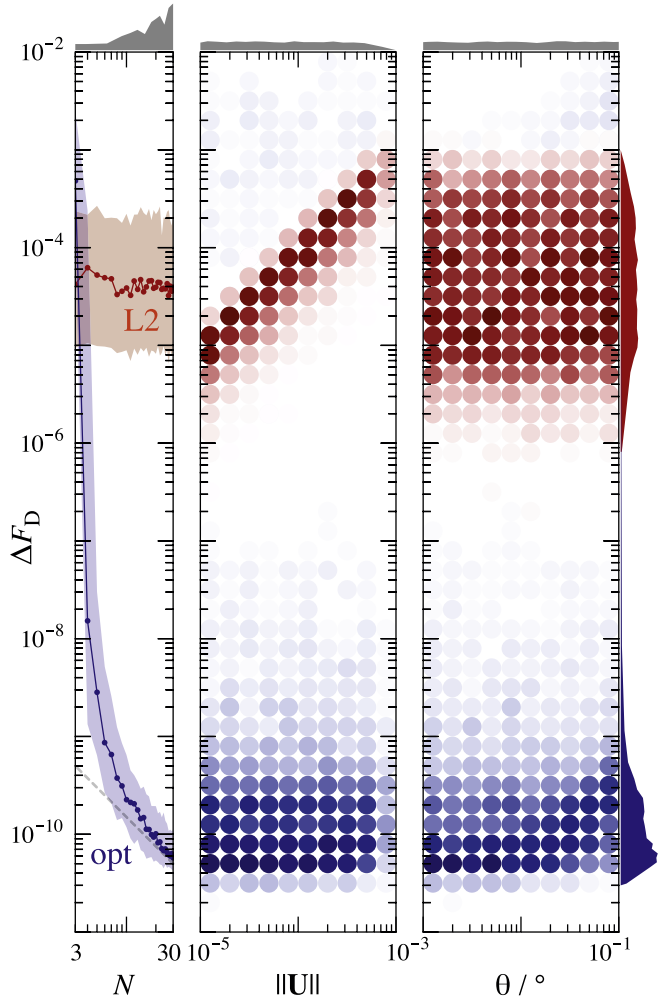

Fig. 2. Reconstruction accuracy of the deviatoric lattice deformation gradient extracted from regular micro-Laue diffraction patterns ($n = 0$) with the L2 and opt methods as a function of the number N of indexed peaks (left), the lattice stretch magnitude $\|\mathbf{U}\|$ (middle), and the incremental lattice rotation angle θ (right). Shaded band in left diagram corresponds to standard deviation around median value illustrated by solid line. Middle and right diagrams depict probability density maps on a logarithmically equi-spaced grid. Distribution of underlying data is presented in the top and right margin.

DAXM experiment, $N \in [3, 30]$ wavevectors are randomly selected out of those detected, where a bias towards lower (h, k, l) mimics the indexation outcome from beamline 34-ID-E. Furthermore, a random fraction of n/N of the indexed wavevectors are assigned a known wavelength, such that the absolute length of their associated scattering vector(s) can be identified.

The N indexed diffraction peaks are termed a "regular micro-Laue diffraction pattern" if all scattering vectors are of unit length, *i.e.*, $n = 0$ scattering vector lengths are known, as would be the case under polychromatic DAXM conditions. In contrast, an "augmented micro-Laue diffraction pattern" contains $n > 0$ scattering vectors for which the exact length is identified (in reality by performing n additional energy scans).

Full (or deviatoric) lattice deformation gradients were extracted from 92108 augmented (or 5527 regular) micro-Laue diffraction patterns using L2 and opt. The resulting accuracy of lattice strain reconstruction was quantified by the magnitude (Frobenius norm) of the deviation,

$$\Delta F = \left\| \check{\mathbf{F}} - \mathbf{F} \right\| \tag{8a}$$

$$\text{and} \quad \Delta F_{\mathrm{D}} = \left\| \check{\mathbf{F}}_{\mathrm{D}} - \mathbf{F}_{\mathrm{D}} \right\|, \tag{8b}$$

between the extracted (full or deviatoric) deformation gradient and the prescribed one.

Fig. 2 compares the reconstruction accuracy of both methods applied to regular micro-Laue diffraction patterns, *i.e.* under white-beam conditions, as function of the number of indexed peaks N, the magnitude $\|\mathbf{U}\|$ of the stretch component, and the lattice orientation deviation angle θ. The direct inversion method L2 produces deviations ΔF_{D} that fall in the same range as the selected stretch magnitudes $10^{-5} \leq \|\mathbf{U}\| \leq 10^{-3}$. The deviations show no notable dependence on either N or θ but exhibit a strong scaling with $\|\mathbf{U}\|$.

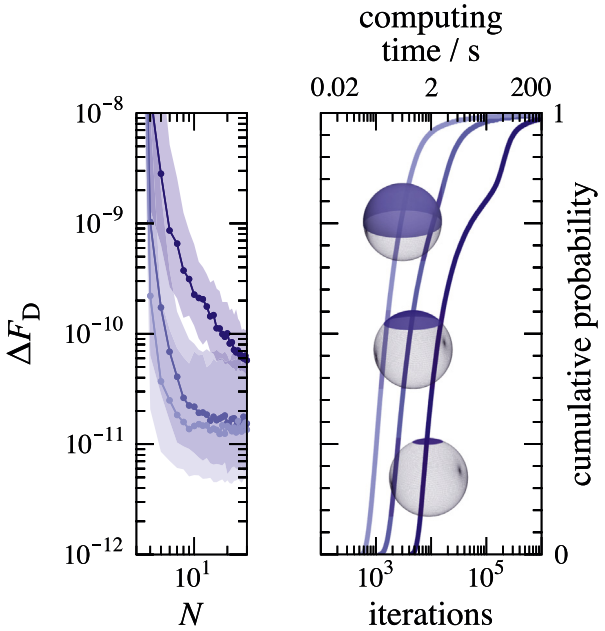

Fig. 3. Reconstruction accuracy (left) and cumulative distribution of the number of iterations required (right) to extract the deviatoric lattice deformation gradient from about 10^4 sets of scattering vectors using opt with different virtual detector sizes having cone angles of 45°, 90°, or 180°(from dark to light blue). Computing times were measured for an implementation based on Scientific Python (scipy 0.19.0) running in single-thread mode on a 14-core 2.4 GHz Intel Xeon E5-2680v4. (For interpretation of the references to color in this figure legend, the reader is referred to the web version of this article.)

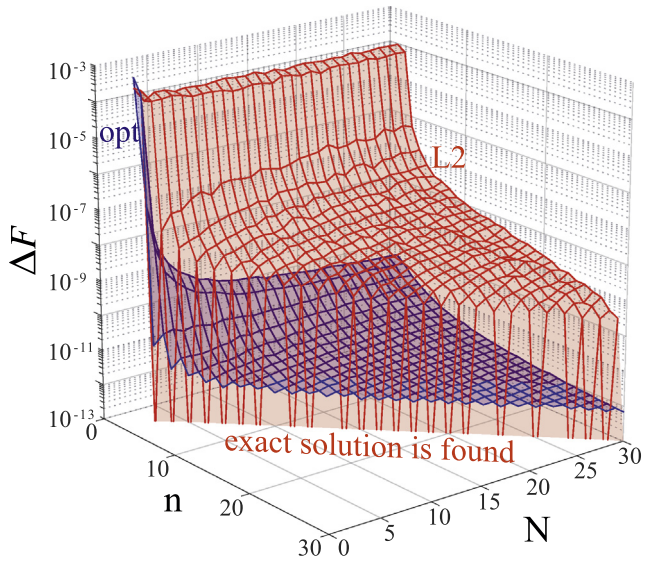

Fig. 4. Reconstruction accuracy of the full lattice deformation gradient resulting from the L2 and opt methods (red and blue) as a function of the number N of indexed peaks and the number $n \in [1, N]$ of peaks with known length, *i.e.*, for which an energy scan is available. (For interpretation of the references to color in this figure legend, the reader is referred to the web version of this article.)

This direct relation between the amount of lattice stretch and the accuracy of its determination is understandable, as under white-beam conditions the individual correction factors in Eq. (6) are inherently $q_0^{(i)}/q^{(i)} - 1 \equiv 0$, while the true value is bound by $\|\mathbf{U}\|$. In contrast, the deviation between prescribed and identified lattice deformation gradient values reconstructed by the opt method is essentially insensitive to both $\|\mathbf{U}\|$ and θ, *i.e.*, to the quantities that are to be identified, but is strongly sensitive to N. With increasing N, the deviation ΔF_D rapidly drops to around 10^{-9} and continues to decrease further, approaching an inverse proportionality $\Delta F_D \propto N^{-1}$ close to $N = 30$ (dashed line in Fig. 2 left). According to these results, the accuracy achievable for the present 34-ID-E detector size and for typical numbers N of indexed peaks should be better than 10^{-9}, which is well below the accuracy limit of 10^{-6} to 10^{-4} asserted by Hofmann et al. [10] based on an argument of limited coverage of reciprocal space associated with small detector sizes.

To investigate the influence of detector size on the reconstruction accuracy that is attainable by the opt method, two virtual detectors larger than the current one installed at beamline 34-ID-E are imagined such that the detected scattering vectors cover a correspondingly larger solid angle. While only limited improvement in accuracy to about 10^{-11} results (Fig. 3 left), the number of objective function (Eq. (7)) iterations expended by the opt method does notably decrease with increasing detector size (Fig. 3 right). More specifically, the typical computation time to optimize the lattice deformation gradient decreases by a factor of about 3 when increasing the detector cone angle from 45° (34-ID-E detector geometry) to 90°, and by another factor of about 3 when increasing the cone angle further to 180°. The practicality of substantially increasing the present detector size is, however, debatable given the complications associated with proper alignment of multiple smaller detectors and current limitations in large-area detector technology.

Determination of the full lattice deformation gradient based on augmented micro-Laue diffraction patterns (white-beam DAXM with additional energy scans, Fig. 4) demonstrates an advantage of opt over L2 similarly to the observations in the white-beam case. The opt method quickly saturates at reconstruction accuracies $\Delta F < 10^{-11}$ for $n \geq 3$, while the L2 method is typically about a factor 10^3 less accurate — with the exception of $n = N$. In other words, when all scattering vectors have known length, such as in the case of high-energy X-ray diffraction microscopy (HEDM), the L2 method can provide the exact solution, whereas the opt method consistently provides very accurate estimates with $\Delta F \approx 10^{-12}$ over a wide range of N and n.

Acknowledgments

This research was supported by the U.S. Department of Energy, Office of Science, Office of Basic Energy Sciences, through grant DE-FG02-09ER46637 and in part by Michigan State University through computational resources provided by the Institute for Cyber-Enabled Research.

References

[1] T.B. Britton, A.J. Wilkinson, Ultramicroscopy 111 (8) (2011) 1395–1404. https://doi.org/10.1016/j.ultramic.2011.05.007.
[2] A.J. Allen, M.T. Hutchings, C.G. Windsor, C. Andreani, Adv. Phys. 34 (4) (1985) 445–473. https://doi.org/10.1080/00018738500101791.
[3] D.A. Hall, A. Steuwer, B. Cherdhirunkorn, T. Mori, P.J. Withers, J. Appl. Phys. 96 (8) (2004) 4245–4252. https://doi.org/10.1063/1.1787590.
[4] J.D. Almer, S.R. Stock, J. Struct. Biol. 152 (1) (2005) 14–27. https://doi.org/10.1016/j.jsb.2005.08.003.
[5] V. Biju, N. Sugathan, V. Vrinda, S.L. Salini, J. Mater. Sci. 43 (4) (2008) 1175–1179. https://doi.org/10.1007/s10853-007-2300-8.
[6] N. Jia, Z.H. Cong, X. Sun, S. Cheng, Z.H. Nie, Y. Ren, P.K. Liaw, Y.D. Wang, Acta Mater. 57 (13) (2009) 3965–3977. https://doi.org/10.1016/j.actamat.2009.05.002.
[7] J.K. Edmiston, N.R. Barton, J.V. Bernier, G.C. Johnson, D.J. Steigmann, J. Appl. Crystallogr. 44 (2) (2011) 299–312. https://doi.org/10.1107/S0021889811002123.
[8] B.C. Larson, W. Yang, G.E. Ice, J.D. Budai, J.Z. Tischler, Nature 415 (6874) (2002) 887–890. https://doi.org/10.1038/415887a.
[9] A. Poshadel, P. Dawson, G. Johnson, J. Synchrotron Radiat. 19 (2) (2012) 237–244. https://doi.org/10.1107/S0909049511050400.
[10] F. Hofmann, B. Abbey, W. Liu, R. Xu, B.F. Usher, E. Balaur, Y. Liu, Nature Commun. 4 (2013) 2774 EP. https://doi.org/10.1038/ncomms3774.